Journal of Volcanology and Geothermal Research 462 (2025) 108322

Contents lists available at ScienceDirect

Journal of Volcanology and Geothermal Research

journal homepage: www.journals.elsevier.com/journal-of-volcanology-and-geothermal-research

Hydrogeochemical processes governing the origin, mobility and transport of trace elements in the Domuyo Volcanic complex Geothermal system (Patagonia, Argentina)

Joaquin Llano[a,b,**], Lorenza Li Vigni[c,*], Mariano Agusto[a,b], Lorenzo Brusca[d], Alberto Caselli[e], Giovanni Chiodini[f], Walter D'Alessandro[d], Matteo Lelli[g,h], Franco Tassi[i,j], Orlando Vaselli[i,j], Sergio Calabrese[c,d,*]

[a] *Universidad de Buenos Aires, Facultad de Ciencias Exactas y Naturales, Departamento de Geologia, Grupo de Estudio y Seguimiento de Volcanes Activos (GESVA), Buenos Aires, Argentina*
[b] *Instituto de Estudios Andinos "Don Pablo Groeber" (IDEAN), Universidad de Buenos Aires – CONICET, Buenos Aires, Argentina*
[c] *Dipartimento di Scienze della Terra e del Mare – DiSTeM, Università di Palermo, Palermo, Italy*
[d] *Istituto Nazionale di Geofisica e Vulcanologia – Sezione di Palermo, Palermo, Italy*
[e] *Instituto de Investigación en Paleobilogía y Geología, Universidad Nacional de Río Negro – CONICET, General Roca, Argentina*
[f] *Istituto Nazionale di Geofisica e Vulcanologia – Sezione di Bologna, Bologna, Italy*
[g] *CNR-IGG Consiglio Nazionale delle Ricerche, Istituto di Geoscienze e Georisorse, Pisa, Italy*
[h] *Istituto Nazionale di Geofisica e Vulcanologia – Sezione di Pisa, Pisa, Italy*
[i] *Università degli Studi di Firenze, Firenze, Italy*
[j] *CNR-IGG Institute of Geosciences and Earth Resources, Florence, Italy*

ARTICLE INFO

Keywords:
Water-gas-rock interaction
Hydrogeochemistry
Geothermal system

ABSTRACT

The system of Domuyo Volcanic Complex is one of the most promising geothermal fields of Patagonia (Argentina). In this paper, we present a geochemical model of the Domuyo geothermal system based on previous studies and integrated with the systematic characterization of trace elements, thus adding a new piece to the puzzle of one of the most impressive geothermal systems in Argentina. A total of 38 water samples were collected from 17 different sampling sites, during three field-campaigns from 2013 to 2016, and analysed for 28 trace elements (Li, Be, B, Al, Ti, V, Cr, Mn, Fe, Co, Ni, Cu, Zn, As, Se, Rb, Sr, Y, Zr, Mo, Cd, Sb, Cs, Ba, Tl, Pb, Th and U). Sampling sites included the main river (Varvarco), its tributaries which cross the geothermal area, and thermal and cold springs. The investigation was focused on the origin, behaviour and estimation of mass fluxes of trace elements. Computing mass fluxes of trace elements transported by rivers is an important tool in the estimation of both the impact of potentially toxic elements and the exploitation of economically valuable elements. Among others, the mass fluxes of trace elements originating from the Domuyo geothermal system transported by rivers range from 45 to 278 t y^{-1} for As, B, Cs, Li, Sr and Rb; such contributions flow to the Varvarco river, where the concentrations and mass fluxes of these elements increase by one to two orders of magnitude in the site downstream of the geothermal area with respect to that upstream.

1. Introduction

The study of trace elements in geothermal systems related to active volcanoes can provide valuable information to understand the dynamic of water-rock interaction processes occurring in the system, define its maturity and magmatic fluid inputs, and, finally, its geothermal potential (Smith et al., 1987; Giggenbach, 1991; Symonds et al., 1992; Deely and Sheppard, 1996; Giammanco et al., 1998; Aiuppa et al., 2000; Delmelle and Bernard, 2000; Taran et al., 2008; Rouwet et al., 2009; Calabrese et al., 2011; Zelenski et al., 2014; Kalacheva et al., 2015).

* Correspondence to: Sergio Calabrese, Lorenza Li Vigni, Dipartimento di Scienze della Terra e del Mare – DiSTeM, Università di Palermo, Palermo, Italy.
** Correspondence to: Joaquin Llano, Universidad de Buenos Aires, Facultad de Ciencias Exactas y Naturales, Departamento de Geologia, Grupo de Estudio y Seguimiento de Volcanes Activos (GESVA), Buenos Aires, Argentina.
E-mail addresses: joaquinllano28@gmail.com (J. Llano), lorenza.livigni@unipa.it (L.L. Vigni), sergio.calabrese@unipa.it (S. Calabrese).

https://doi.org/10.1016/j.jvolgeores.2025.108322
Received 7 January 2025; Received in revised form 21 March 2025; Accepted 24 March 2025
Available online 27 March 2025

In Argentina, trace elements studies from geothermal systems have rarely been investigated, mostly including only a few elements (Panarello, 2002; Peralta Arnold et al., 2017; Wrage et al., 2017; Chiodi et al., 2019; Tardani et al., 2021; Rojas et al., 2022; Llano et al., 2022; Llano et al., 2023; Chiodi et al., 2024). Although the study of trace elements is of extreme interest both for environmental issues, contamination by potentially toxic metals in the different matrices, and for the possible recovery and exploitation of valuable geo-resources (such as Lithium or technological critical elements), the Domuyo geothermal system has never been characterized, either in terms of its lithology or its hydrological system.

The Domuyo Volcanic Complex has been recognized as one of the most promising geothermal resources in the Argentinian territory (JICA, Japan International Cooperation Agency, 1983; JICA, Japan International Cooperation Agency, 1984; Panarello et al., 1992; Pesce, 2013; Tassi et al., 2016), whose potential energy release was evaluated in ~1 GW (Chiodini et al., 2014). Nevertheless, detailed studies on the chemical composition of the Domuyo waters, including the characterization of trace elements, are lacking to date. With the aim of filling this gap, in this study, the water geochemistry of the Domuyo Volcanic Complex (including major ions and 28 minor/trace elements) was investigated. Three field campaigns were carried out in 2013, 2014, and 2016, when 38 samples of natural waters have been collected from 17 sampling sites, including surface waters, thermal and cold springs. Additionally, the flow rates of the main rivers were also measured. The main aims were to: i) investigate the geochemical processes occurring within the geothermal reservoir and its associated shallow hydrological system; ii) evidence the contribution of a deep magmatic source (e.g., B, As, Tl, and Sb; Calabrese et al., 2011; Scholtysik and Canil, 2018; Mandon et al., 2019; Inostroza et al., 2022) as well as a mature geothermal brine (e.g., Li, Rb, and Cs; Taran et al., 2008; Kaasalainen and Stefánsson, 2012; Kalacheva et al., 2017; Li Vigni et al., 2023); iii) quantify the mass flow of major and trace elements from the geothermal area to the main river in order to evaluate its environmental impact and iv) compute the thermal energy release from the geothermal reservoir. The overall aim was to fill an important gap in the scientific literature on this extreme environment by providing a previously unpublished database on water, which may serve as a basis for future work in the fields of geothermics, environmental geochemistry, biogeochemistry, water resource exploitation and mineral georesources.

1.1. Regional setting

1.1.1. Geological setting

Along the South American Andean range, four zones with active volcanoes have been recognized, three of them been distributed along the Argentina-Chile boundary (Stern, 2004). The Domuyo Volcanic Complex (36°34′S, 70°25′W, DVC hereafter) is the highest mountain in Patagonia (4702 m a.s.l.) and is located in the transitional segment of the South Volcanic Zone (latitude 33°S - 46°S). This complex (Fig. S1) has a rock basement formed by Permo-Triassic sandstones, conglomerates, and pyroclastic deposits, named as Choiyoi Group (Groeber, 1947; Zappettini et al., 2012; Galetto et al., 2018), which were intruded by granodioritic bodies belonging to the Varvarco Formation (Llambías, 1986; JICA, Japan International Cooperation Agency, 1992; Pesce, 2013; Silva-Fragoso et al., 2021). Above the Permo-Triassic basement, low metamorphosed ignimbrites (Primavera Formation) and the lower part of the Neuquén basin sedimentary sequence, represented by shales, evaporites, limestones, and fine sandstones (Pesce, 1981; Silva-Fragoso et al., 2021), occur. Tertiary rocks are constituted by the Charilehué Formation, which are volcaniclastic deposits of pumice and ash flows, basaltic to andesitic flows, and ignimbrites (Burns et al., 2006; Silva-Fragoso et al., 2021). Another Tertiary deposit in the region belongs to the Manchana Covunco Formation which comprises basaltic to andesitic flows dated from 4.0 ± 0.42 to 2.85 ± 0.38 Ma (Pesce, 2013; Silva-Fragoso et al., 2021). DVC was shaped by the emplacement of different domes referable to voluminous explosive and effusive activity from 2.5 ± 0.5 to 0.254 ± 0.023 Ma (JICA, Japan International Cooperation Agency, 1983; Pesce, 1983; Miranda, 1996). To the east of DVC, a rhyolitic dome with dacitic flows (Cerro Domuyo) occurs, whereas the Domuyo volcaniclastic sequence is characterized by different pyroclastic and ash deposits (Silva-Fragoso et al., 2021). Finally, regarding igneous rocks, mafic lava flows emmited from monogenetic cinder cones are located at the western side of the Varvarco river and the south area of Cerro Domuyo, with Pleistocene or Holocene ages (Silva-Fragoso et al., 2021).

The main structures in the area are controlled by tectonic inversion developed over normal faults that form a basin, originated from late Triassic to early Jurassic times (Fig. S1; Galetto et al., 2018).

1.1.2. Hydrological system

The hydrological system of the DVC is composed by different river drainage. The Varvarco river is the main watercourse and is located 10 to 12 km to the west of Cerro Domuyo, flowing N-S and being mainly fed to the east by permanent and ephemeral tributaries (Fig. 1). Some authors (Pesce, 1983; Galetto et al., 2018; Silva-Fragoso et al., 2021; Godoy et al., 2023) have proposed that the *E*-W faults from the Miocene graben control the path of the main tributaries of the Varvarco river, e.g. Manchana Convunco, Aguas Calientes, and Covunco rivers. These rivers are fed by precipitation and snow melting (JICA, Japan International Cooperation Agency, 1984; Falaschi et al., 2022) as well as by thermal and cold springs located along their riverbeds (Fig. 1; Villalba et al., 2020). The main thermal springs are El Humazo, Las Ollitas, Aguas Calientes, and Los Tachos, all of them reaching temperature > 90 °C, i.e. boiling temperature at the emergence outlet (1700–2100 m a.s.l.) and presenting vigorously boiling at the discharging point (Chiodini et al., 2014; Tassi et al., 2016; D'Elia et al., 2020; Villalba et al., 2022). The thermal manifestations are located in the mentioned Miocene graben, allowing the up-flow of steam, hot water, and geothermal gases from the N-S lineament known as Manchana-Covunco normal fault (Galetto et al., 2018; Godoy et al., 2023). In this geothermal field argillic and phyllic to argillic alteration is recognized, especially in El Humazo thermal spring (Mas et al., 2000). However, the most remarkable fluid emissions, known as La Bramadora (an ~15 m high vapor column), is located at ~3150 m a.s.l., SW of Cerro Domuyo and comprises vapor columns and boiling pools with acidic gas emissions (Tassi et al., 2016).

In the northern part of the geothermal field is located the Ahilinco river, fed by a thermal spring known as Las Papas that reaches up to 40 °C (Fig. 1; Tassi et al., 2016). In contrast, other rivers sited in the southern part are not affected by thermal springs and discharge into the Varvarco river; these include the Atreuco, Matanzilla, Chagay, and Manzano rivers.

1.1.3. The DVC geothermal reservoir

The geothermal field is located in the Miocene graben boundaries and is fed by a reservoir located between 400 and 800 m (Pesce, 2013; Tassi et al., 2016), probably in the highly fractured Miocene rocks, with water temperatures from 220 to 250 °C (Panarello et al., 1992; Chiodini et al., 2014; Tassi et al., 2016). Water recharge comes from meteoric precipitation in the upper parts of the NW sector of Cerro Domuyo (JICA, Japan International Cooperation Agency, 1984). Meteoric waters, once infiltrated into the aquifer with a short residence time (Tassi et al., 2016), heat up rapidly due to the magmatic source and rise to surface trough the Manchana Covunco fault and the *E*-W trending faults that cross the geothermal field (Galetto et al., 2018; Godoy et al., 2021). It is important to mention that some authors have hypothesized the possibility of a second gas-dominated aquifer located at a depth of 2 to 3 km (Tassi et al., 2016; Lundgren et al., 2020), where volcano-tectonics events occur probably related to the Manchana Covunco fault and favoured by the mobility of deep magmatic gases (Godoy et al., 2021; Godoy et al., 2023).

The heat source of the geothermal system is associated with the

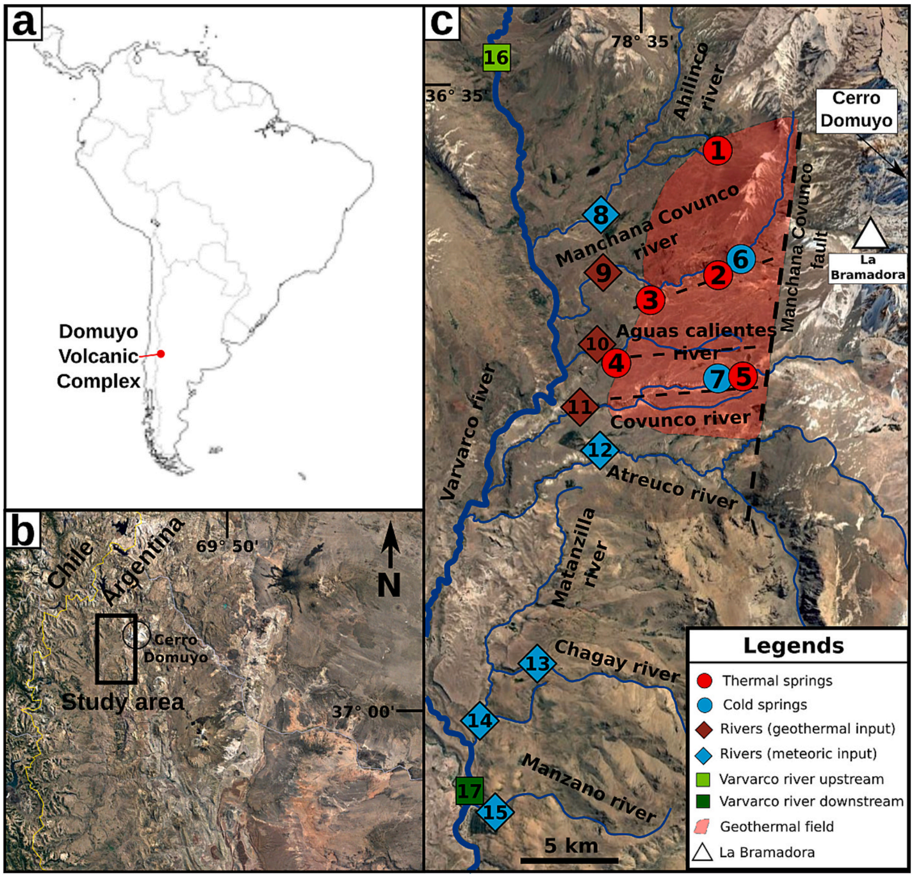

Fig. 1. a) and b) Location of the Domuyo Volcanic Complex, c) its hydrographic system on the eastern flank and the sampling sites (site reference in Table 1). Thermal springs in red dots: 1) Las Papas; 2) El Humazo; 3) Las Olletas; 4) Aguas Calientes; 5) Los Tachos. Cold springs in light blue dots: 6) El Humazo; 7) Los Tachos. Rivers (with geothermal input in brown diamonds,with meteoric input in light blue: 8) Ahilinco; 9) Manchana Covunco; 10) Aguas Calientes; 11) Covunco; 12) Atreuco; 13) Chagay; 14) Matanzilla; 15) Manzano; 16) Varvarco upstream in light green square; 17) Varvarco downstream in green square.

Pleistocene rhyolitic magmatic chamber (0.6 to 0.2 Ma) centred below La Bramadora surface manifestations (SW of Cerro Domuyo; Pesce, 2013; Silva-Fragoso et al., 2021) at 6 to 7 km depth (Lundgren et al., 2020; Godoy et al., 2021) or 4 to 6 km depth (Astort et al., 2019). These authors suggest that the magma chamber has a considerably large volume, about 200 km^3, which requires hundreds of thousands of years to cool down. Nevertheless, new magma might have accumulated more recently without reaching the surface, being this evidenced in the 12 cm y^{-1} to 15 cm y^{-1} inflation of Cerro Domuyo region (Astort et al., 2019; Lundgren et al., 2020), until the year 2019 (Derauw et al., 2020).

As previously mentioned, the DVC geothermal field has been described as one of the most promising geothermal fields in the world. The thermal energy released was estimated to be 1.1 ± 0.2 GW by Chiodini et al. (2014), basing on the chloride fluxes measured at the thermal springs. The high thermal energy release is also testified by the hydrothermal eruptions that have affected the El Humazo area (D'Elia et al., 2020 and references therein).

1.2. Methodology

1.2.1. Sampling sites

Three field campaigns were carried out in 2013, 2014, and 2016 during the summer season (February–March), and 38 natural water samples were collected from 17 different sampling sites (Fig. 1 and Table 1). All the data presented are unpublished, except for the major ions from the 2014 campaign (Tassi et al., 2016).

In the geothermal field, thermal water emissions are boiling and bubbling pools mostly located on the foothills of Cerro Domuyo (Fig. 1),

Table 1
Geographical location of the sampling sites.

ID	Sample site	Latitude (UTM)	Longitude (UTM)	Altitude (m a.s.l.)	Type
1	Las Papas	361,278	5,947,250	2166	Thermal spring
2	El Humazo	361,002	5,942,747	1991	Thermal spring
3	Las Olletas	358,400	5,941,715	1870	Thermal spring
4	Aguas Calientes	356,511	5,939,451	1762	Thermal spring
5	Los Tachos	361,901	5,938,273	2043	Thermal spring
6	El Humazo cold spring	361,866	5,942,377	2198	Cold spring
7	Los Tachos cold spring	361,906	5,938,262	2050	Cold spring
8	Ahilinco river	356,191	5,945,057	1658	River
9	Manchana Covunco river	355,626	5,942,334	1585	River
10	Aguas Calientes river	356,362	5,939,441	1739	River
11	Covunco river	354,135	5,936,607	1541	River
12	Atreuco river	355,327	5,935,187	1668	River
13	Chagay river	353,923	5,926,988	1474	River
14	Matanzilla river	350,995	5,924,804	1301	River
15	Manzano river	350,748	5,921,130	1252	River
16	Varvarco river upstream	352,305	5,950,486	1581	Main river
17	Varvarco river downstream	350,368	5,921,396	1184	Main river

where also fumaroles of different vapor fluxes can be observed. Las Papas samples (Site 1) were collected from bubbling pools situated near a creek of a small stream. El Humazo (Site 2; Fig. 2a) is an area near Manchana Covunco river where there are boiling pools of 2 to 3 m diameter, hot springs, mud pools, and fumaroles with vapor emissions up to 15 m high. Las Ollitas thermal spring (Site 3) forms part of an area where there are bubbling and boiling pools with vapor emissions up to 10 m high (Fig. 2b). Aguas Calientes thermal spring (Site 4; Fig. 2c) is located 2 km upstream the confluence between Aguas Calientes river and Varvarco river. The last sample corresponding to the thermal spring is Los Tachos (Site 5; Fig. 2d). Both cold springs sampled, El Humazo (Site 6) and Los Tachos (Site 7), are close to the homonymous thermal springs. Ahilinco river (Site 8) is fed by Las Papas thermal spring, whereas Manchana Covunco (Site 9; Fig. 2e) receives the discharges of El Humazo cold and thermal springs. Instead, Aguas Calientes river (Site 10) is fed by Aguas Calientes thermal spring. Finally, Covunco river (Site 11), receives the discharge of both cold and thermal springs of Los Tachos (Fig. 1).

Moving down to the south of the geothermal area, streams not affected by discharging thermal manifestations (Fig. 1), such as Atreuco river (Site 12), Chagay river (Site 13), Matanzilla river (Site 14), and Manzano river (Site 15) were also sampled.

The Varvarco river drains in the study area from North to South (Fig. 1) and, as it is fed by the previously mentioned tributaries, two samples were taken on this river, one upstream (Site 16) ~12 km before the confluence with the first river draining trough the geothermal field (Ahilinco river), and a second sample downstream (Site 17; Fig. 2f), a few tens of meters after the Manzano river flows into the main watercourse.

1.2.2. Field measurements, sampling methods, and laboratory analysis

Physicochemical parameters (temperature, pH, and electrical conductivity) were measured in situ using a portable multiparameter instrument (HANNA HI 991301). Filtered (at 0.45 μm) samples were collected in 250 mL plastic bottles for anions analysis (SO_4^{2-}, HCO_3^-, CO_3^{2-} Cl^-, F^-, Br^-) and in 150 mL plastic bottles for cations (Na^+, K^+, Ca^{2+}, Mg^{2+}); a 50 mL aliquot for trace elements was sampled in pre-washed vials. Both two aliquots, for cations and for trace elements, were acidified with ultrapure HNO_3 until reaching a pH <2.

The water samples collected in 2013 for the determination major ions content were analysed in the laboratories of the Istituto Nazionale di Geofisica e Vulcanologia of Palermo (INGV – PA), presented in this work, and of Istituto Nazionale di Geofisica e Vulcanologia - Osservatorio Vesuviano in Naples (INGV – OV), published in Chiodini et al. (2014). The difference between each lab results was <5 % (comparison can be found in Supplementary Materials Table S2). Major ions and trace elements of the water samples collected in 2014 and 2016 were analysed at the laboratories of the INGV - PA.

Anions were determined by ion chromatography (ICS-1100, Dionex), while total alkalinity (mostly HCO_3^- and CO_3^{2-}) was determined on the field by acidimetric titration with HCl 0.1 N, using a microdosimeter and methyl-orange as pH-indicator. The detection limits were 0.01 mg L^{-1} for Cl^-, F^-, SO_4^{2-}, Br^-, CO_3^{2-}, and HCO_3^-. Cations were analysed by ion chromatography (ICS-1100, Dionex) and the detections limits were 0.01 mg L^{-1} for Mg^{2+} and 0.05 mg L^{-1} for K^+, Ca^{2+}, and Na^+. The analytical errors were ≤ 5 % for all the species. Trace elements were analysed by inductively coupled plasma mass spectrometer (ICP-MS) using an Agilent 7500ce instrument, with precision always better than 3 %. Calibration solutions for all investigated elements were prepared daily using

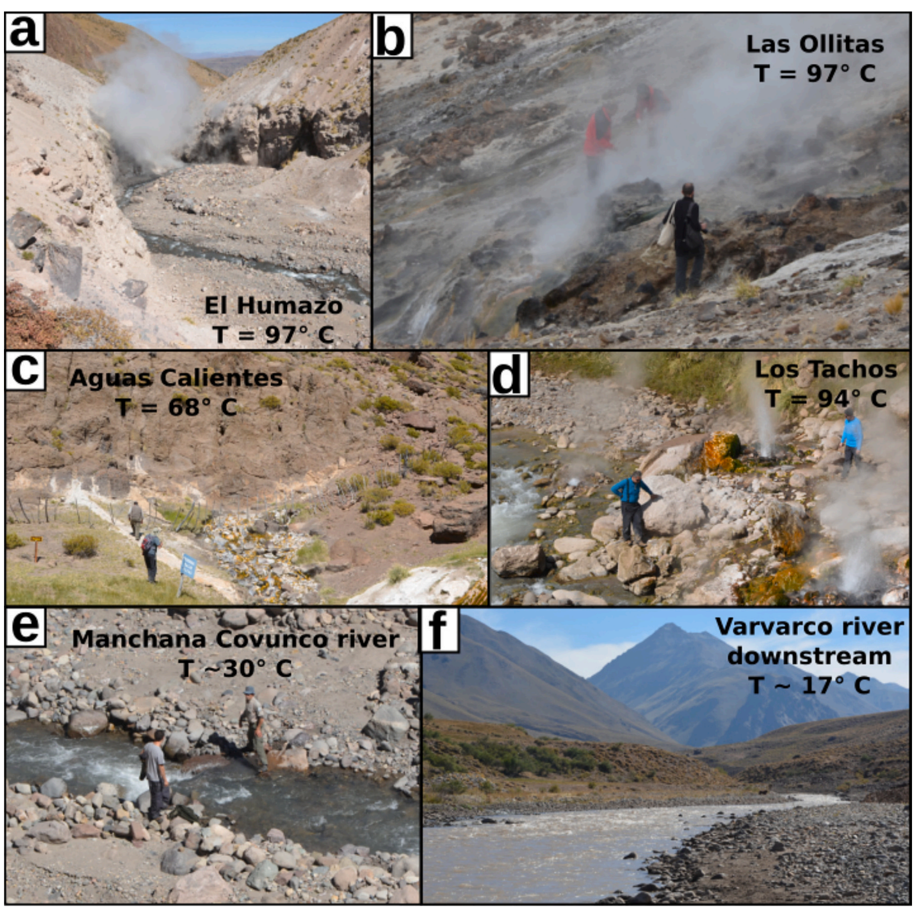

Fig. 2. a) El Humazo thermal manifestation and Manchana Covunco river (site 2). b) Las Ollitas geothermal area (site 3). c) Aguas Calientes thermal spring (site 4). d) Los Tachos geothermal area (site 5). e) Manchana Covunco river sampling site (site 9). f) Varvarco River downstream (site 17).

an appropriate dilution of 100 mg L^{-1} and 1000 mg L^{-1} of stock standard solutions (Merck) with 0.14 mol L^{-1} high-purity nitric acid.

The quality assurance and quality control (QA/QC) procedures included field and analytical blanks, cleaning procedures, and inter-laboratory comparison between Istituto Nazionale di Geofisica e Vulcanologia (INGV-PA) and Osservatorio Vesuviano in Naples (INGV – OV). In addition, some samples (three in each campaign) were analysed as duplicates to check for reproducibility, and reagent blanks were analysed with samples to check baseline contamination. All the blanks collected in the field (Millipore water) showed results below detection limit for most of the trace elements or, in a few cases, negligible concentrations were recorded when compared to the analysed samples. The analytical accuracy of trace element determinations was checked by the analysis of four Certified Reference Materials (TM Rain 04, SLR4, SLRS5, SPSSW1).

Flow rates results of Chiodini et al. (2014) were used for 2013 campaign values, whereas the same method was used in the 2014 survey for flow rate calculation of the upper and lower reaches of the Varvarco river, Ahilinco, Manchana Covunco, Aguas Calientes, Covunco, and Atreuco rivers. Eventually, during the 2016 survey the flow measurements were performed using a mobile acoustic flow meter for measurement of point velocities according to the method of verticals. The device was indeed also equipped with an integrated pressure sensor to measure both current water level at each vertical and the immersion depth of the sensor. The accuracy of velocity and water level sensors are 1 % and 0.1 % of measured value, respectively. The computed flow rates were then used to calculate the fluxes of major and trace elements for the 3-years surveys.

1.2.3. Estimation of thermal energy release

The thermal energy release $Q_{(H)}$ of Domuyo geothermal field, expressed in GW, was computed by (i) determining the flux of geothermal chloride (Q_{Cl}), using the river chloride inventory method proposed by Fournier et al. (1975), and (ii) by estimating the original chloride concentration (Cl_T) and enthalpy (H_T - kJ kg^{-1}) of the geothermal brine at the estimated reservoir temperature, as follows:

$$Q_{(H)} = (Q_{Cl}/Cl_T) \text{ x } H_T \quad (1)$$

Q_{Cl}, expressed in g s^{-1}, is given by the difference between the fluxes of chloride in the downstream and upstream river of the hot water inflow, computed by multiplying the chloride content by the respective flow rates measured at Varvarco river.

The Cl_T (g kg^{-1}) was calculated by following mass balance equation (Marini and Cioni, 1985).

$$Cl_T = Cl_0/(1-x) \quad (2)$$

where Cl_0 is the median value of the chloride concentrations in all studied thermal springs, whereas x is the steam fraction. In this work, the steam fraction at 100 °C was considered, resulting in the maximum steam loss. Lastly, the enthalpy value was determined through the estimation of the temperature of the geothermal reservoir, as outlined in Giggenbach (1988).

2. Results

2.1. Physicochemical parameters and major ions

Temperature, pH, electrical conductivity (EC), and major ions concentrations of the 2013, 2014, and 2016 samples are listed in Supplementary Materials (Table S1), whereas average, maximum, and minimum values of these results are listed in Table 2. As shown in Fig. 3, the temperature and EC clearly shows the differences between the different types of water sampled, which can be distinguished in: i) thermal springs with high temperature (40–97 °C) that can reach near boiling values for these altitudes (1800 to 3200 m a.s.l.) and high EC (3810–11,768 μS cm^{-1}); ii) rivers fed by thermal fluids (Aguas calientes, Manchana Covunco and Covunco rivers) with intermediate temperature (21–48 °C) and intermediate to high EC (1900–5860 μS cm^{-1}). The

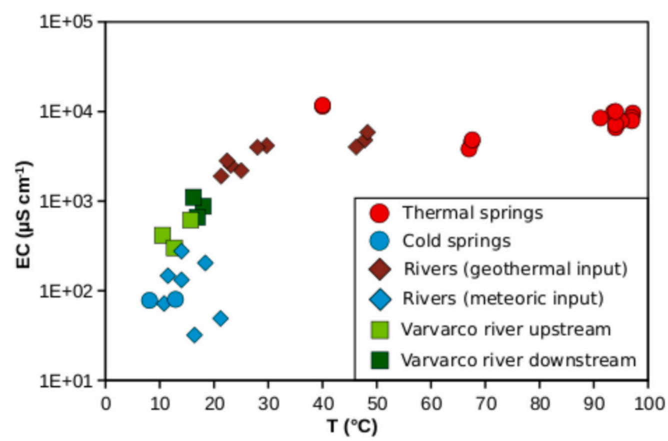

Fig. 3. Electrical conductivity (EC) vs temperature where it is recognized the difference among each group of water.

Table 2
Statistical values of chemical compositions of the 2013, 2014, and 2016 samples assembled in the six water groups.

Site		T	pH	EC	HCO_3^-	CO_3^{2-}	SO_4^{2-}	Cl^-	F^-	Br^-	Na^+	K^+	Ca^{2+}	Mg^{2+}
	Average	81	7.5	8012	286	0.064	166	1631	3.46	6.24	1110	83	73	9.56
Thermal springs	Minimum	40	6.1	3810	78	0.064	77	863	1.17	2.93	609	43	24	0.25
	Maximum	97.2	8.3	11,768	1281	0.064	308	2470	5.94	11	1690	152	271	60
	Average	10.5	6.8	79	21	n.a.	2.27	9.74	0.16	n.a.	8.41	1.45	3.95	0.82
Cold springs	Minimum	8.1	6.8	78	15	n.a.	1.39	0.36	0.05	n.a.	2.98	1.40	3.74	0.54
	Maximum	12.9	6.8	80	28	n.a.	3.15	19	0.27	n.a.	13	1.50	4.16	1.09
	Average	32.4	8.2	3580	117	1.14	177	709	1.93	2.34	488	43	68	3.42
Rivers with geothermal input	Minimum	21.3	7.2	1900	74	0.96	62	475	1	1.35	302	30	24	1.57
	Maximum	48.3	8.9	5860	166	1.98	332	1045	2.95	3.58	705	63	132	5.2
	Average	15.2	8	130	50	6.30	2.71	6.69	0.17	0.016	8.42	2.11	8.3	3.07
Rivers with meteoric input	Minimum	10.8	6.9	32	15	6.30	0.7	0.50	0.05	0.016	3.14	0.82	3.14	0.56
	Maximum	21.2	9.4	276	95	6.30	6.18	20	0.29	0.016	18	3.9	14	5.00
	Average	13	8.2	443	70	0.82	137	2.47	0.16	n.a.	5.07	1.69	67	2.74
Varvarco river upstream	Minimum	10.5	7.9	300	56	0.82	131	1.43	0.09	n.a.	4.15	1.38	65	2.49
	Maximum	15.7	8.6	614	90	0.82	143	4.27	0.27	n.a.	5.7	2.2	69	3.01
	Average	17	7.9	880	75	n.a.	136	130	0.43	0.55	91	10	64	3.04
Varvarco river downstream	Minimum	16.2	7.7	660	56	n.a.	123	105	0.39	0.35	70	8.14	58	2.90
	Maximum	18	8	1104	93	n.a.	151	145	0.5	0.86	108	12	71	3.20

Temperature (T) are in °C, electrical conductivity (EC) are in μS cm^{-1}, and ion concentrations are in mg L^{-1}. n.a. is not analysed, n.d. is not detected.

Varvarco river that presents low temperatures (10–18 °C), but can be distinguish between iii) upstream and iv) downstream by its EC (300–614 µS cm^{-1} and 660–1104 µS cm^{-1}, respectively); v) rivers only fed by meteoric waters; vi) cold springs with low temperatures (8–21 °C) and low EC (78–276 µS cm^{-1}).

Las Papas thermal spring has a pH around 6.0, whereas Aguas Calientes thermal spring has a pH from 6.7 to 6.9. The remaining thermal springs (El Humazo, Las Ollitas, and Los Tachos) have pH that vary between 7.7 and 8.3. The anions concentrations in the thermal springs (Fig. 4 and Table 2) present average values of 286 mg L^{-1} for HCO_3^-, of 1631 mg L^{-1} for Cl^-, of 166 mg L^{-1} for SO_4^{2-}, of 3.5 mg L^{-1} for F^-, and 6.2 mg L^{-1} for Br^-. The average cations concentrations are of 1110 mg L^{-1} for Na^+, 82 mg L^{-1} for K^+, 9.5 mg L^{-1} for Mg^{2+}, and 73 mg L^{-1} for Ca^{2+}.

The El Humazo and Los Tachos cold springs, present pH of 6.8 and have low average ionic compositions (Fig. 4 and Table 1; HCO_3^-: 21 mg L^{-1}; Cl^-: 9.7 mg L^{-1}; SO_4^{2-}: 2.2 mg L^{-1}; F^-: 0.16 mg L^{-1}; Br^-: <d.l.; Na^+: 8.4 mg L^{-1}; K^+: 1.4 mg L^{-1}; Ca^{2+}: 3.9 mg L^{-1}; Mg^{2+}: 0.82 mg L^{-1}).

The rivers fed by thermal manifestations (Manchana Covunco, Aguas Calientes, and Covunco) show pH values from 7.2 to 8.8, and average ion compositions (Fig. 4 and Table 2) for HCO_3^- of 117 mg L^{-1}, Cl^- of 709 mg L^{-1}, SO_4^{2-}, of 177 mg L^{-1}; F^- of 1.9 mg L^{-1}, Br^-, of 2.3 mg L^{-1}, Na^+ of 488 mg L^{-1}, K^+, of 43 mg L^{-1}, Ca^{2+} of 68 mg L^{-1}, Mg^{2+} of 3.4 mg L^{-1}. On the other hand, the rivers only fed by meteoric water (Chagay, Ahilinco, Atreuco, Matanzilla, and Manzano) present neutral to alkaline pH (6.8–9.4), and have low average ions concentrations (HCO_3^-: 49 mg L^{-1}; Cl^-: 6.7 mg L^{-1}; SO_4^{2-}: 2.7 mg L^{-1}; F^-: 0.17 mg L^{-1}; Br^-: <d.l.; Na^+: 8.4 mg L^{-1}; K^+: 2.1 mg L^{-1}; Ca^{2+}: 8.3 mg L^{-1}; Mg^{2+}: 3 mg L^{-1}). In this last group, the surface waters of Ahilinco river are included despite being fed by Las Papas thermal spring, since the latter is apparently limited to a relatively low contribution of Cl^- concentrations (17–20 mg L^{-1}).

The Varvarco river upstream presents similar average pH value (8.2) to the rivers not affected by thermal discharges with comparable main ion concentrations (HCO_3^-: 70 mg L^{-1}; Cl^-: 2.5 mg L^{-1}; F^-: 0.16 mg L^{-1}; Br^-: <d.l.; Na^+: 5.1 mg L^{-1}; K^+: 1.7 mg L^{-1}; Mg^{2+}: 2.7 mg L^{-1}), except for SO_4^{2-} and Ca^{2+}, that present much higher average concentrations (137 mg L^{-1} and 67 mg L^{-1}; respectively). In Varvarco river downstream, although pH and some average ions concentrations almost do not vary significantly (pH: 7.9; HCO_3^-: 75 mg L^{-1}; SO_4^{2-}: 136 mg L^{-1}; F^-: 0.43 mg L^{-1}; K^+: 10 mg L^{-1}; Ca^{2+}: 64 mg L^{-1}; Mg^{2+}: 3.0 mg L^{-1}), the Cl^- and Na^+ average concentrations considerably increase (129 mg L^{-1} and 91 mg L^{-1}, respectively).

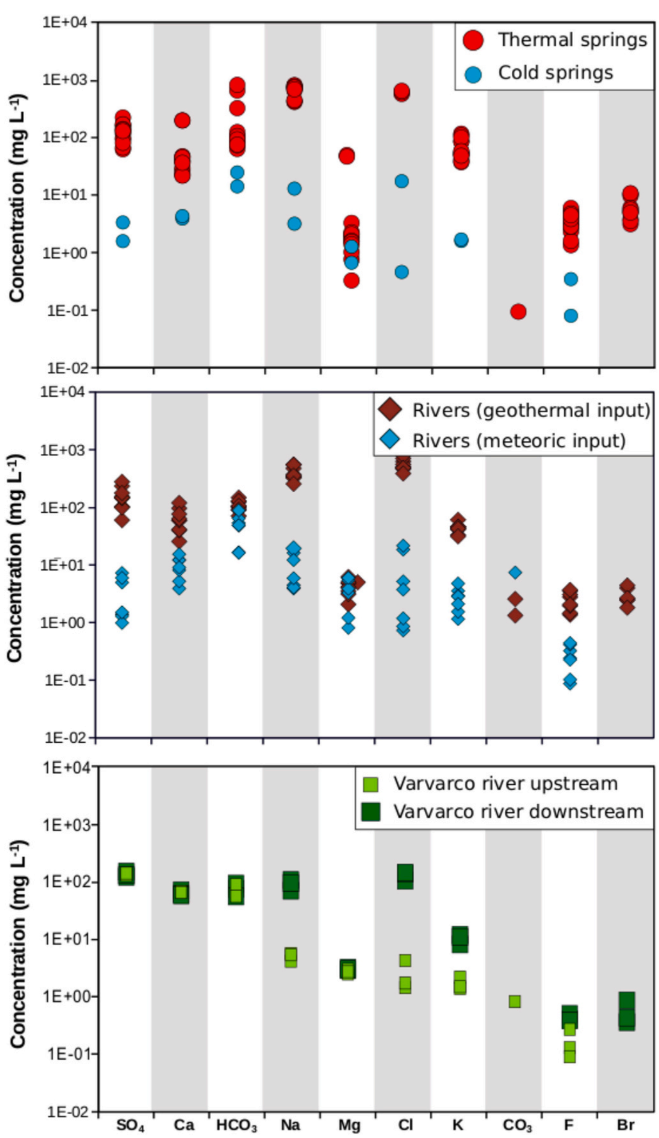

Fig. 4. Main ionic concentrations in all the samples arranged for decreasing values at Varvarco river upstream.

2.2. Trace elements

Trace element concentrations are listed in Supplementary Materials (Table S1) and summarized in Table 3 and Fig. 5. The highest contents of trace elements in the thermal springs refer to Li, B, As, Rb, Sr, and Cs (580–13,000 µg L^{-1}). Other elements such as Al, Ti, Mn, Fe, Zn, Mo, Sb, Ba, V, and Tl have concentrations between 0.9 and 430 µg L^{-1}, whereas Be, Cr, Co, Ni, Cu, Se, Y, Zr, Cd, Pb, Th, and U show abundances from <0.001 to 4.5 µg L^{-1}. Exception is Las Papas springs that shows lower concentrations for Mo (0.5–1 µg L^{-1}), V (0.2–0.3 µg L^{-1}), and Tl (0.65–0.75 µg L^{-1}), and higher concentration of Be (4.9–5.5 µg L^{-1}) and Fe (3600–4000 µg L^{-1}).

In the cold springs the concentrations of Li, B, Al, Ti, Mn, Fe, Zn, As, Rb, Sr, Cs, and Ba vary from 1.1 to 630 µg L^{-1}, except for Li, B, and Cs in the El Humazo cold spring as these elements present lower concentrations (<0.001–0.3 µg L^{-1}). The rest of the trace elements (Be, V, Cr, Co, Ni, Cu, Se, Y, Zr, Mo, Cd, Sb, Tl, Pb, Th, and U) have contents below 1 µg L^{-1}.

The rivers fed by thermal manifestations have similar trace elements concentrations to the thermal springs. Lithium, B, As, Rb, Sr, and Cs have concentrations from 420 to 6400 µg L^{-1}, whereas elements such as Al, Ti, Mn, Fe, Zn, Mo, Sb, V, Ba, and Tl from 0.5 to 92 µg L^{-1}. Other trace elements (Be, V, Cr, Co, Ni, Cu, Se, Y, Zr, Cd, Pb, Th, and U) are always below 0.5 µg L^{-1}.

Rivers not fed by thermal manifestations have concentrations from 1.8 to 60 µg L^{-1} for B, Al, Mn, Fe, Zn, Sr, and Ba. Lower contents were measured for Li, Ti, V, Ni, Cu, As, Mo, Cs, and Rb (between 0.1 and 3 µg L^{-1}), except for Ahilinco river since Li and Rb have concentrations from 6.8 to 55 µg L^{-1}; Be, Cr, Co, Se, Y, Zr, Mo, Cd, Sb, Tl, Pb, Th, and U display a concentration range between <0.001–0.9 µg L^{-1}.

The Varvarco river presents similar concentrations in some elements in both upstream and downstream sampling sites: Al, Mn, Fe, Sr, and Ba are indeed varying from 5 and 600 µg L^{-1}, whereas Be, Ti, Cr, Co, Ni, Cu Zn, Se, Y, Zr, Cd, V, Mo, Th, and U show concentrations up to 2.4 µg L^{-1}. However, some elements present enrichment in their average concentrations after the mixing with the geothermal field tributaries: Li (5.0 µg L^{-1} to 763 µg L^{-1}), B (12 µg L^{-1} to 703 µg L^{-1}), As (1.3 µg L^{-1} to 148 µg L^{-1}), Rb (3.2 µg L^{-1} to 113 µg L^{-1}), Sb (0.06 µg L^{-1} to 7.5 µg L^{-1}), Cs (0.07 µg L^{-1} to 105 µg L^{-1}), and Tl (0.019 µg L^{-1} to 0.68 µg L^{-1}).

2.3. Flow rates

The flow rates of the investigated rivers are shown in Table S3 with

Table 3
Statistical values of trace elements of the 2013, 2014, and 2016 samples assembled in the six water groups.

Site		Li	Be	B	Al	Ti	V	Cr	Mn	Fe	Co	Ni	Cu	Zn	As
Thermal springs	Average	9640	1.12	8457	29	18	3.30	0.98	161	576	0.54	0.89	1.11	9.93	2006
	Minimum	5158	0.038	4797	2.64	7.66	n.d.	n.d.	2.48	1.73	n.d.	0.044	0.068	1.56	951
	Maximum	12,831	5.56	11,531	114	38	11.6	3.46	428	3932	4.55	5.69	3.41	27	2877
Cold springs	Average	101	0.01	86	10	1.09	0.49	0.064	53	324	0.33	0.17	0.25	6.91	7.14
	Minimum	101	n.d.	n.d.	10	1.06	0.18	0.057	1.88	15	n.d.	0.079	0.24	3.67	1.47
	Maximum	101	0.012	86	11	1.12	0.80	0.071	104	632	0.33	0.26	0.27	10	12
Rivers with geothermal input	Average	4754	0.14	4236	35	13	2.96	0.21	28	35	0.20	0.60	0.36	11	922
	Minimum	2753	0.044	2391	7.57	5.05	0.52	n.d.	13	9.27	0.026	0.21	0.067	2.16	558
	Maximum	6363	0.27	5507	91	23	7.24	0.43	43	91	0.42	2.03	0.65	27	1298
Rivers with meteoric input	Average	15	0.0037	36	23	2.29	0.91	0.19	35	57	0.20	0.70	0.45	15	1.60
	Minimum	0.46	n.d.	7.11	11	0.94	0.25	0.035	5.07	1.14	0.003	0.11	0.14	2.21	1.07
	Maximum	54	0.0043	74	59	4.34	1.60	0.88	95	91	0.81	3.03	1.36	29	2.34
Varvarco river upstream	Average	5.07	0.013	12	31	1.62	0.80	0.13	10	24	0.17	0.37	0.26	5.81	1.33
	Minimum	3.98	n.d.	6.61	12	0.38	0.76	n.d.	6.65	5.06	0.12	0.18	0.22	1.79	1.15
	Maximum	6.25	0.013	16	41	2.68	0.83	0.16	15	59	0.21	0.59	0.32	10	1.49
Varvarco river downstream	Average	763	0.020	703	67	11	1.66	0.30	21	35	0.49	0.47	1.44	21	148
	Minimum	640	0.0037	563	38	2.20	1.29	0.079	8.06	21	0.32	0.34	1.01	5.30	125
	Maximum	845	0.047	805	107	23	2.39	0.56	38	62	0.65	0.59	2.24	49	170

Site		Se	Rb	Sr	Y	Zr	Mo	Cd	Sb	Cs	Ba	Tl	Pb	Th	U
Thermal spring	Average	0.17	1046	1646	0.27	0.046	8.80	0.13	77	1520	100	5.84	0.22	0.080	0.096
	Minimum	n.d.	497	389	0.13	0.012	0.57	0.025	9.10	909	19	0.65	n.d.	0.0012	n.d.
	Maximum	0.24	1997	5796	1.17	0.11	16	0.70	128	2110	321	16	0.82	0.50	0.33
Cold spring	Average	0.10	9.49	20	0.060	0.031	0.54	0.012	0.29	6.72	4.97	0.019	0.079	0.0018	0.0080
	Minimum	0.084	4.29	14	0.034	0.011	0.10	0.010	0.039	0.34	2.17	1.014	0.078	0.0010	0.0023
	Maximum	0.11	14	25	0.085	0.052	0.97	0.014	0.54	13	7.77	0.024	0.081	0.0026	0.013
Rivers with geothermal input	Average	0.21	603	946	0.10	0.018	6.63	0.042	35	792	39	3.92	0.17	0.018	0.18
	Minimum	n.d.	425	511	0.018	0.0096	4.95	0.012	20	446	26	2.25	n.d.	0.0008	0.15
	Maximum	0.29	848	1752	0.46	0.026	8.80	0.086	56	1188	50	6.75	0.54	0.091	0.22
Rivers with meteoric input	Average	0.098	3.34	56	0.037	0.080	0.50	0.034	0.050	0.57	8.02	0.0076	0.10	0.0013	0.025
	Minimum	n.d.	1.30	13	0.024	0.026	0.27	0.015	0.024	0.082	1.86	0.0032	0.022	0.0003	0.0021
	Maximum	0.10	8.02	88	0.051	0.18	0.76	0090	0.11	1.97	14	0.014	0.33	0.0024	0.052
Varvarco river upstream	Average	0.16	3.22	464	0.028	0.0075	1.69	0.035	0.069	0.078	11	0.019	0.042	0.0011	0.070
	Minimum	0.15	2.98	402	0.027	0.0075	1.60	0.029	0.060	0.043	9.95	0.0069	0.039	0.0011	0.063
	Maximum	0.17	3.44	512	0.030	0.0075	1.78	0.046	0.079	0.14	13	0.036	0.048	0.0011	0.078
Varvarco river downstream	Average	0.16	113	553	0.048	0.024	2.29	0.11	7.47	105	21	0.68	0.55	0.034	0.094
	Minimum	0.12	95	486	0.034	0.024	2.08	0.037	5.83	83	20	0.48	0.16	0.0006	0.089
	Maximum	0.19	128	596	0.063	0.024	2.46	0.23	8.68	120	21	0.81	0.95	0.069	0.10

Concentrations are in μg L^{-1}. n.a. is not analysed, n.d. is not detected.

an error estimated between 10 and 25 %. The higher average flow rate belongs to the Varvarco river upstream (6077 L s^{-1}), followed by Manchana Covunco river (1260 L s^{-1}) and Covunco river (1053 L s^{-1}), whereas Atreuco and Ahilinco river present flow rates of 330 and 240 L s^{-1}, respectively. Finally, Aguas Calientes river provides 84 L s^{-1}. All these flow rates sum 8637 L s^{-1}, i.e. a lower value than that measured in the Varvarco river downstream (11,790 L s^{-1}). The flow rate variability recorded in the three surveys may be due to the changes of winter precipitations (Falaschi et al., 2022).

3. Discussion

The thermal springs show a Na^+-Cl^- composition (Fig. 6) typical of mature geothermal fluids (e.g. Giggenbach, 1991). Some rivers show a Na^+-Cl^- composition, being fed by these thermal manifestations, whereas others have a Ca^{2+}/Na^+-HCO_3^-(Cl^-) composition, including those not relevantly affected by thermal manifestations. Noteworthy, waters from the Ahilinco and Atreuco rivers, located at the periphery of the geothermal spring area, show intermediate features with respect to the previous two compositional facies. Consequently, some rivers are only supplied by a meteoric input, whereas other rivers are characterized by meteoric and geothermal input. The Ca^{2+}-SO_4^{2-}(HCO_3^-) composition of the upper reaches of the Varvarco river likely corresponds to the local geochemical baseline before the mixing with those rivers that are also fed by notable contributions of Na^+-Cl^- waters (Fig. 6). The concentrations of HCO_3^- and SO_4^{2-} in Varvarco river indicate the possible dissolution of carbonates and gypsum in the upper part of its basin, also reflected in the Ca^{2+} concentrations (Villalba et al., 2022), while the rest of the species come from interactions processes involving silicate rocks.

3.1. Origin and mobility of major ions and trace elements

Temperature and water chemistry of the thermal springs (circum-neutral pH, high EC and high Na^+ and Cl^- concentrations) indicate the contribution from a mature geothermal system. As the geothermal fluids are uprising, they are likely affected by steam separation at shallow depth, causing an increase in pH (ranging from 6.8 to 9.3) due to CO_2 loss (Chiodini et al., 2014). This process is not occurring for the Aguas Calientes and Las Papas thermal springs (pH ranging from 6.1 to 6.8) since they are only suffering a mixing between the geothermal source and a shallow cold groundwater (Chiodini et al., 2014). At Las Papas, HCO_3^-, Cl^-, and all the major cations show higher concentrations relative to those of the other thermal manifestations, likely due to a low mixing with surface waters (Tassi et al., 2016). Carbon dioxide in the associated gas phase is the most important source of HCO_3^- in the thermal waters (Tassi et al., 2016), whereas the relatively high SO_4^{2-} concentrations indicate oxidation of H_2S from the deep hydrothermal system (Tassi et al., 2016). Chloride, F^- and Br^- likely originate from dissolution of HCl, HF and HBr. Low Ca^{2+} concentrations are due to precipitation of carbonates (Tassi et al., 2016; Villalba et al., 2020), whereas very low Mg^{2+} concentrations (ranging from 0.25 to 5.2 mg

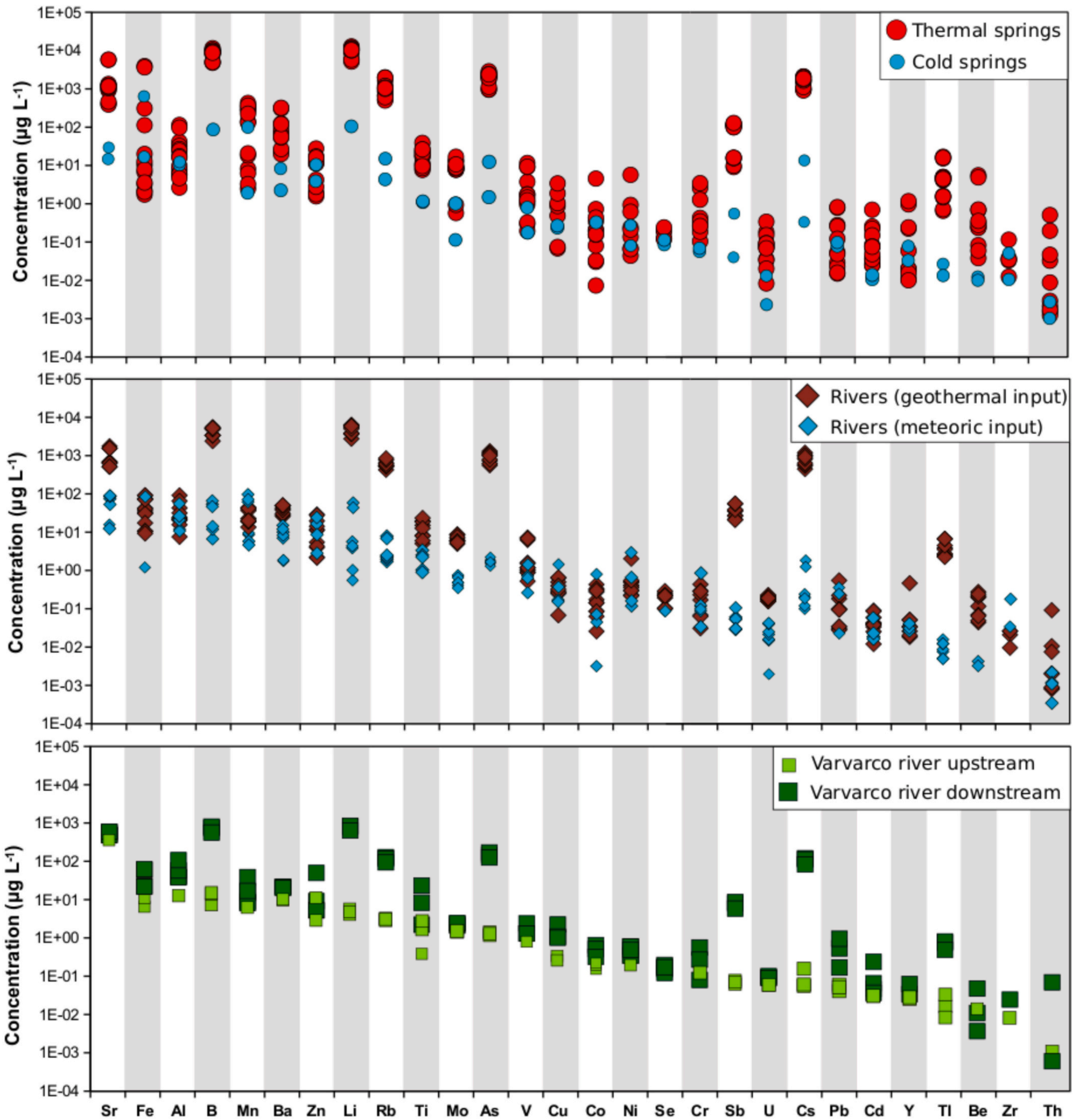

Fig. 5. Trace elements concentrations in all the samples arranged for decreasing values at Varvarco river upstream.

L^{-1}) underscore the high maturity of the waters, being hosted in chlorite formed at geothermal temperatures (Giggenbach, 1988).

The cold springs present low-to-negligible hydrothermal contribution, likely approaching the chemical composition of the water recharging the geothermal system, slightly modified by low-temperature water-rock interaction. Nevertheless, Los Tachos cold spring presents relatively higher concentrations of Na^{+} and Cl^{-} than those of El Humazo cold spring, the former possibly being affected by a slight input from the geothermal waters. The contribution of hydrothermal water into the Manchana Covunco and Covunco rivers was estimated to range from 20 % to 50 %, whereas for Aguas Calientes almost all of the water comes from the hydrothermal system (Villalba et al., 2022).

The average relative mobility ($RM = (C_i/Mg^{2+})_w/(C_i/Mg^{2+})_r$; where C is concentration of each element and subscripts w and r relate to water and rock, respectively) was calculated for the main cations and trace elements from the hot and cold springs, the geothermally affected tributaries, and the Varvarco river (Fig. 7). In these diagrams it can be easily identified which elements are enriched ($RM > 1$) or depleted ($RM < 1$) with respect to Mg^{2+}. The upper continental rock composition from Wedepohl (1995) was used as the normalizer.

The RMs are very similar for all the thermal water samples, except for Las Papas that has lower RMs due to its higher Mg^{2+} concentrations. In the high temperature waters the enrichment in both volatile elements (As, B, Sb, Se, and Tl) and elements that may behave as volatiles (Mo and

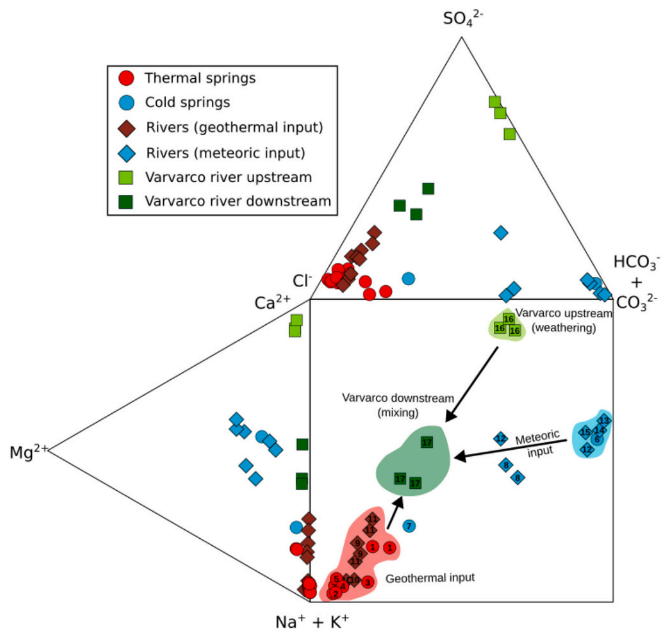

Fig. 6. Durov diagram showing the chemical composition of the DVC geothermal waters and related geochemical processes affecting the surface waters.

Cd) is remarkable. This phenomenon can be attributed to the contribution of magmatic gases and may be enriched by phase separation in the geothermal brine aquifer (Arnórsson and Andrésdóttir, 1995; Calabrese et al., 2011; Kaasalainen and Stefánsson, 2012; Scholtysik and Canil, 2018; Mandon et al., 2019; Inostroza et al., 2022). It is noteworthy to point out that the geothermal brine not only provides species such as Na^+ and Cl^- but also supplies trace elements typical of compositionally mature waters, such as Li, Cs, and Rb (Giggenbach, 1991; Kaasalainen and Stefánsson, 2012; Chiodini et al., 2014; Wrage et al., 2017). Lithium has been observed to be highly soluble and not notably partitioned into secondary minerals (Ellis and Mahon, 1964; Wrage et al., 2017), whereas Cs is too large to substitute other alkali metals in secondary minerals (Ellis and Mahon, 1967). Rubidium instead can be incorporated in K-bearing phases when precipitating (Kaasalainen and Stefánsson, 2012; Wrage et al., 2017) and Sr behaves in the thermal waters similar to Ca^{2+}, tending to replace it in Ca^{2+}-hosted minerals. Beryllium, Mn, Ba, Zn, and V present RMs close to 1, indicating a similar behaviour to Mg^{2+} in these waters. Neutral to alkaline pH waters favor the precipitation of Fe- and Al-hydroxides, that may influence the mobility of other trace elements. Indeed, the co-precipitation of trace elements, such as Ni, Cr, Co, U, Cu, As, Ti, Pb, and Th, can be induced by adsorption processes on these hydroxides (Ellis and Mahon, 1967; Aiuppa et al., 2006; Morales-Simfors et al., 2020), whereas Y, Zr, and Th are prone to be retained in the host rock.

A behaviour similar to the thermal springs for As, B, Li, Cs, Na^+, Sb, Se, and Mo can be recognized in Los Tachos indicating that this cold spring may be also slightly affected by the geothermal fluids. Strontium, Ca^{2+}, Rb, K, Tl, Cd, Zn, and Cu have RMs close to 1, suggesting that their behaviour is similar to that of Mg^{2+}. In the cold springs, Be, Ba, Ni, Cr, U, Ti, Zr, Hf, and Al exhibit depleted values with respect to Mg^{2+} due the formation of secondary minerals, such as barite and different oxides and hydroxides or, more likely, they are recalcitrant to alteration at low temperature. Eventually, El Humazo cold spring presents RMs close to 1 for As, Cs, Na^+, Sb, Sr, Rb, indicating low input from the geothermal brine.

The behaviour of trace elements in the geothermally-fed rivers is almost identical to the thermal springs. Arsenic, B, Li, Cs, Na^+, Sb, Rb, Se, Tl, and Mo have high RM values, whereas those of Sr, Ca^{2+}, Be, Mn, Ba, Ni, Cd, Zn, U, and V are close to 1. Waters from Atreuco river, which is not fed by thermal manifestations, and Ahilinco river, fed by the very low output flux of Las Papas thermal spring, are characterized by RMs of trace elements similar to those of El Humazo cold spring. This may indicate that these rivers are fed mostly by meteoric water originated by snow melting that interact with the rocks of the area. In all the rivers, Fe, Cr, Co, Y, Ti, Pb, Zr, Th and Al present RMs $< < 1$ due to precipitation of hydroxides (Ellis and Mahon, 1967).

Downstream Varvarco river, As, B, Li, Na^+, Sb, Rb, and K^+ present higher RMs than upstream, indicating the income of these elements to the system from the geothermal field rivers, as recognized before. It is important to mention that Se, Mo, and Cd present similar RM values in all the Varvarco river samples, since there is no significant input of these elements from the magmatic gases to the system, and their enrichment in the geothermal manifestations can be explained by high concentrations in the host rocks. The geothermal brine does not significantly contribute to the concentrations of Sr, Ca^{2+}, and Zn which exhibit RMs close to 1. Manganese, Ba, Ni, Co, U, Cu, V, and Pb display RMs < 1 in both sampling sites of the Varvarco river (sites 16 and 17), due to the possible co-precipitation of these elements with or as hydroxides. The low RMs of Fe, Cr, and Al can be explained by precipitation as hydroxides while that of Y, Ti, Zr, and Th indicate that they tend to remain in the rock during the water-rock interaction process.

3.2. Mass balance of major and trace elements

The mass balance of major ions and trace elements in the DVC hydrological system was calculated using the flow rates and the element concentrations for each campaign. Each class of fluxes refers to the four water groups recognized according to the geochemical composition, as follows: i) Varvarco river upstream; ii) Varvarco river downstream; iii) tributaries with geothermal input (Manchana Covunco, Aguas Calientes, and Covunco rivers); and iv) tributaries with only meteoric input (Ahilinco and Atreuco rivers). The results are presented in Fig. 8 and in Supplementary Materials (Table S4).

In the Varvarco river downstream Na^+, Cl^-, and SO_4^{2-} present values between 34,000 to 50,000 t y^{-1} while those of Ca^{2+} and HCO_3^- are comprised between 23,000 to 27,000 t y^{-1}, followed by those of K^+ and Mg^{2+} (3800 and 1100 t y^{-1}, respectively). Lithium, B, Sr, and F^- have fluxes of 159 to 285 t y^{-1}, whereas those of As, Rb, and Cs vary between 39 and 55 t y^{-1}. Fluxes of Al, Fe, Ba, Zn, Mn, Sb, and Ti are lower, ranging from 1.5 to 25 t y^{-1}, whereas Mo, V, Tl, Co, Ni, and Cr have fluxes always below 1 t y^{-1}. Eventually, a few elements (Se, Cu, Cd, Pb, U, and Y) have fluxes below 0.1 t y^{-1}. As average, more than 95 % of the conservative species (such as Cl^-, Na^+, Li, B, Rb, and Cs) in Varvarco river downstream are released by the river tributaries (Manchana Covunco, Aguas Calientes, and Covunco rivers) fed by the geothermal reservoir. The same happens with other elements, despite not being conservative, such as As, Sb, and Tl, where the input to the Varvarco river, in its lower reaches, from the geothermal system represents more than 97 %. Something similar occurs for K^+ and F^-, representing 89 and 78 % of the geothermal input, respectively. Some species (SO_4^{2-}, HCO_3^-, Ca^{2+}, Mg^{2+}, Al, Fe, V, Co, Ni, Cr, Cu, Cd, and Se) present lower input proportions from the geothermally-fed rivers (25 to 40 %). This indicates that the main source of these elements is from the Varvarco river headwaters basin (Zanettini et al., 2001; Pesce, 2013) resulting by chemical weathering. Barium, Sr, Mn, Zn, Mo, Pb, and Y have similar proportions in the input from the geothermally-fed rivers and the Varvarco river upstream (between 40 and 60 % each), which may be explained by leaching of rocks that are presented in both part of the hydrological system. Finally, the contribution of some species from Ahilinco and Atreuco rivers to Varvarco river downstream is not negligible, despite their low flow rates. Iron present contributions of 10.1 %, whereas Mg^{2+}, Cu, V, Cr, Mn, Cd, Pb, Zn, and Y represent between 2 and 5.6 % of the total contribution.

For most species, the sum of the element fluxes from Varvarco river

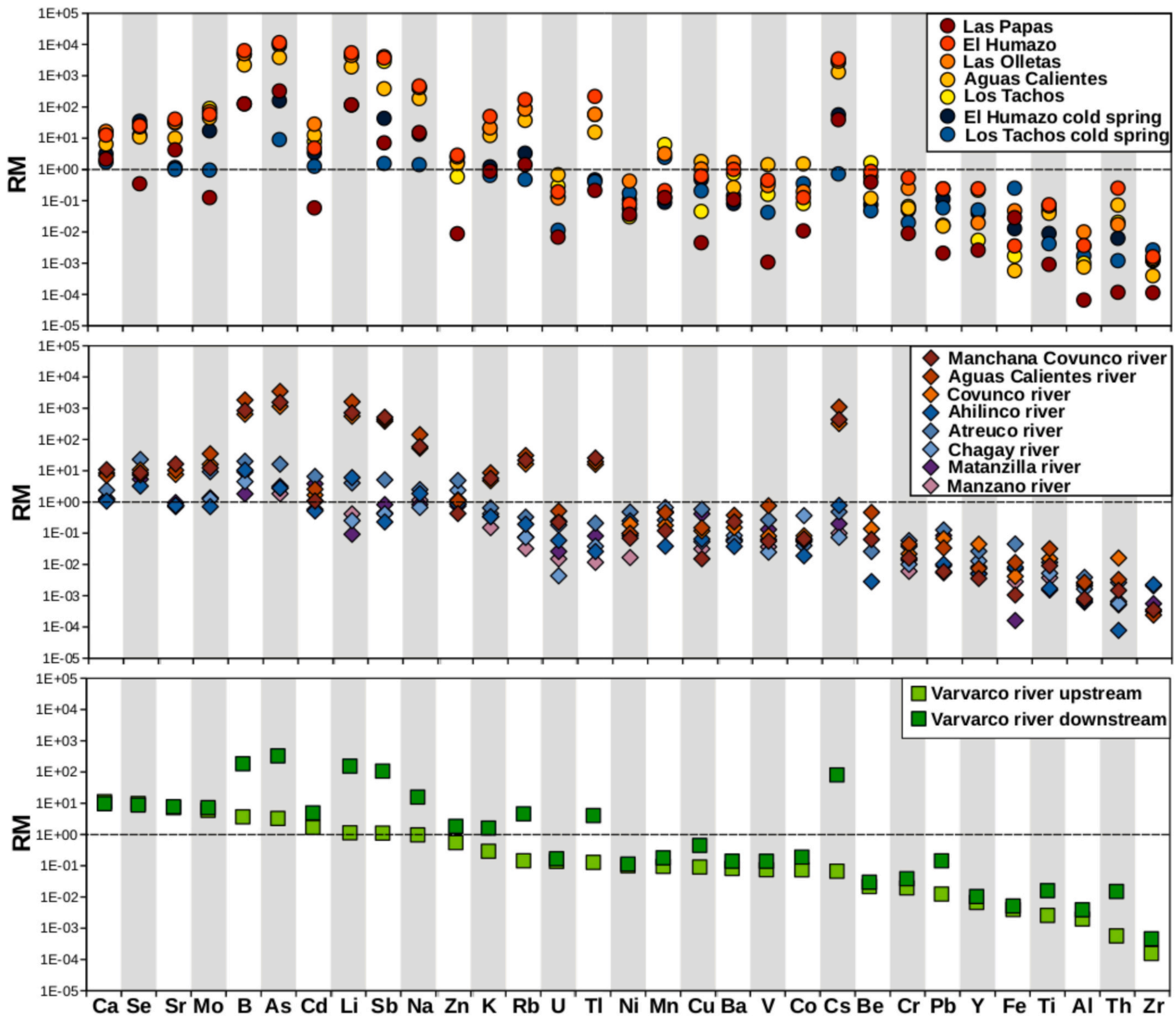

Fig. 7. Average relative mobility (RM) of major cations and trace elements for all the DVC water samples. The normalizer element is Mg^{2+}. Elements are arranged for decreasing values at Varvarco river upstream.

upstream, the geothermally-fed rivers, Ahilinco, and Atreuco rivers is different from those computed downstream (Table S4). These differences range between 5 and 20 % in most solutes (Cl^-, SO_4^{2-}, HCO_3^-, F^-, Na^+, K^+, Ca^{2+}, Mg^{2+}, Sr, Mo, Ni, Se, Ti, U, and Y), and likely related to the flow estimation uncertainty. Some trace elements, such as Li, B, Cu, As, Rb, Sb, Cs, Ba, and Tl, show more notable differences (20 to 50 %) between Varvarco river downstream and the sum of the tributary contribution (including Varvarco river upstream). This can be explained by the possible loss of water from the tributaries due to infiltration into the permeable alluvial deposits and later seeps into the main river downstream to feed the local shallow aquifers (Chiodini et al., 2014; D'Elia et al., 2020; Villalba et al., 2020). Additionally, some of these elements can be affected by precipitation of secondary minerals, thus affecting fluxes in the mass balance calculation for the Varvarco river downstream. Finally, Al, V, Cr, Mn, Fe, Co, Zn, Cd, and Pb are characterized by differences higher than 50 %, reaching up to 300 %, due to higher fluxes in the Varvarco river downstream than in those of the tributaries. Some differences could also be related to direct contribution of geothermal waters in the riverbed, whose presence was however observed. This apparently could be confirmed by the rivers which even if not affected by the main geothermal manifestations (such as the Atreuco and Ahilinco rivers) provide significant contributions of this last group of elements to the main river.

3.3. *Geothermal energy output*

The estimation of the total energy release of Domuyo Volcanic Complex was computed for each year (2013, 2014, and 2016) and compared with the estimation carried out by Chiodini et al. (2014). According to Silva-Fragoso et al. (2021), the DVC high enthalpy geothermal reservoir is located at a depth of 2 km, having been sealed by a volcaniclastic sequence and silicic lavas. The authors propose that the above-calculated high enthalpy is attributable to the presence of a large cooling magma intrusion within the magmatic chamber.

The eq. (1) was solved considering the flow rates of Varvarco river upstream and downstream for each year (Table S5), and an original chloride concentration of the geothermal liquid of 1.31 ± 0.01 g kg^{-1}. Lastly, the enthalpy was calculated for an original reservoir temperature

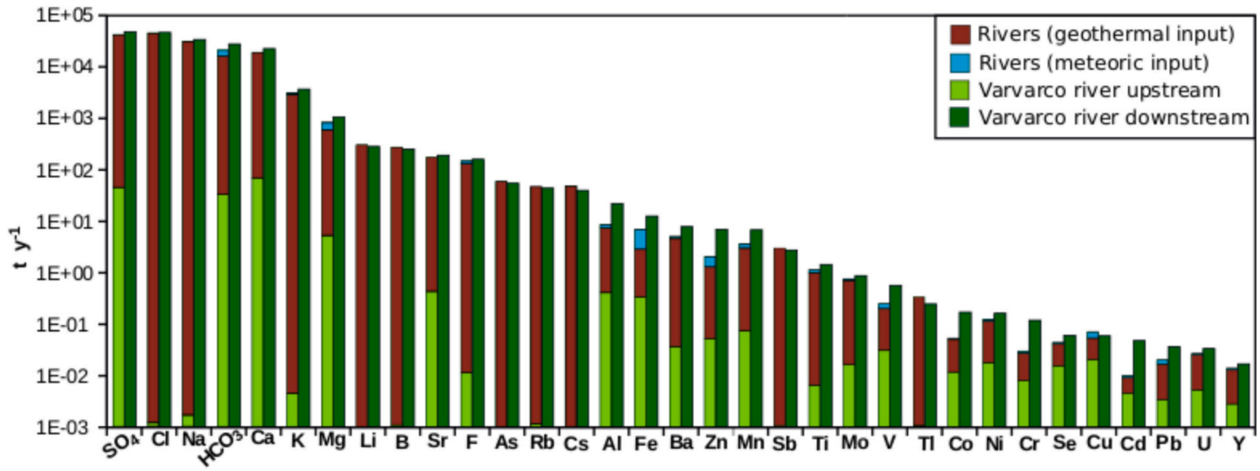

Fig. 8. All species average fluxes (t y^{-1}) from the main rivers are indicated separately. Rivers with geothermal input includes Manchana Covunco, Aguas Calientes, and Covunco rivers, whereas rivers with meteoric input refer to Ahilinco and Atreuco rivers. Species are arranged for decreasing values at Varvarco river downstream.

of 200 ± 20 °C, based on the water and gas geothermometric computation carried out by Chiodini et al. (2014) and Tassi et al. (2016).

The computation gives values of the total energy output of 1.3 ± 0.2 GW for 2013, 1.1 ± 0.2 GW for 2014, and 0.8 ± 0.2 GW for 2016, with an average value of 1.0 ± 0.2 GW. Although comparable to the estimates provided by Chiodini et al. (2014), i.e. 1.1 ± 0.2 GW, the latter value is slightly lower due to the relevant influence in the measurements of the river flow rates for the chloride mass balance calculation. Nevertheless, these energy outputs represent an important advective heat flux, confirming that DVC system remains an extensive reservoir with a considerable geothermal energy potential.

3.4. Geochemical conceptual model

The characteristics of the Domuyo Volcanic Complex geothermal system and the main geochemical processes that are involved are summarized and outlined in the geochemical conceptual model proposed of Fig. 9 (modified from Tassi et al., 2016). A very large cooling magmatic chamber, located between Cerro Domo and Cerro Covunco at depths ranging from 4 to 7 km (Astort et al., 2019; Lundgren et al., 2020; Godoy et al., 2021; Silva-Fragoso et al., 2021), releases elevated heat fluxes and an enormous amount of CO_2- and ^{3}He-rich fluids (Panarello et al., 1992; Chiodini et al., 2014; Tassi et al., 2016) that interact with a mature

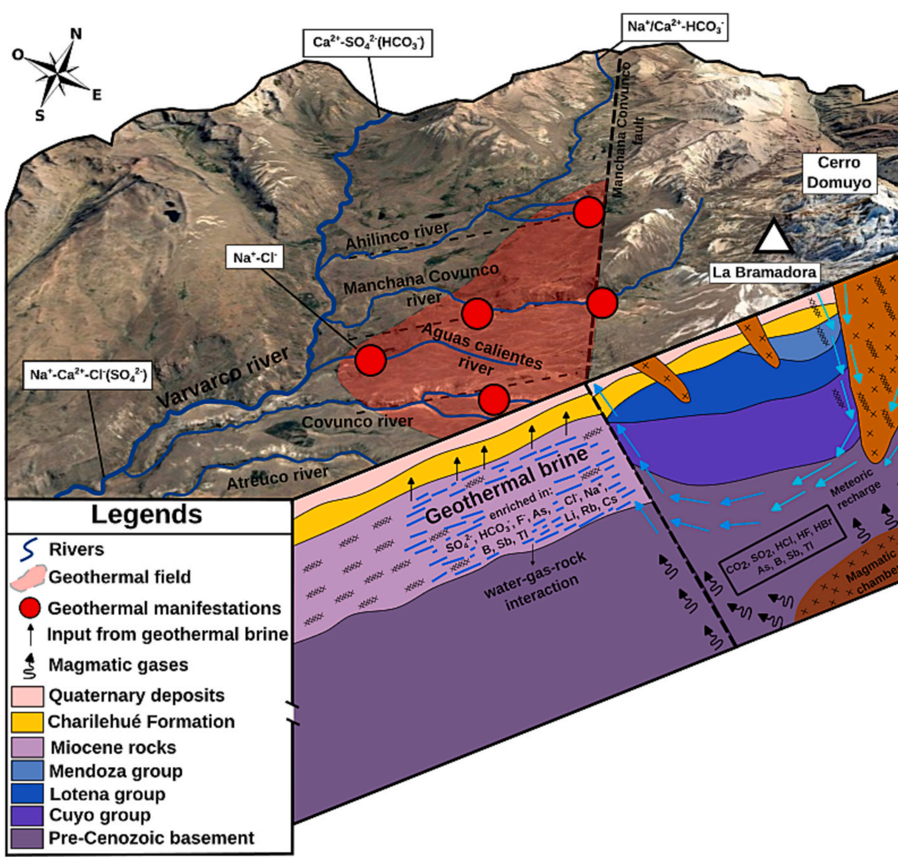

Fig. 9. Schematic model of the Domuyo Volcanic Complex hydrological system and related processes. The stratigraphy is based on the study by Galetto et al., 2018.

geothermal brine. According to Tassi et al. (2016), the water recharge of the geothermal system derives by local rain and melting snow that infiltrate in the NW sector of Cerro Domuyo. During water-gas-rock interaction processes, the magmatic gases dissolve into the hydrothermal aquifers providing to the brine species such as SO_4^{2-}, Cl^-, HCO_3^-, F^-, As, B, Sb, and Tl, whilst the interaction between the deep fluids and the hosting rocks favor reducing conditions, leading to the production of H_2S, CO, and CH_4 (Tassi et al., 2016). Lastly, the progressive rock leaching enriches the brine in Cl^-, Na^+, Li, Rb, and Cs.

These processes that control the geochemical features of thermal fluids uprising are driven by the structural setting of the area. The N-S trending Manchana Covunco fault is likely the preferred path for rising magmatic gases (e.g. CO_2, SO_2, HCl, HF, HBr) and the infiltrated heated waters, whereas the *E*-W trending faults that cross the geothermal field promote the fluids ascent from the geothermal reservoir to the surface (Galetto et al., 2018).

The thermal springs, thus, represent the result of above-mentioned processes. Indeed, the gas are characterized by high concentration of hydrothermal gas and by magmatic isotopic signature (Tassi et al., 2016). On the other hand, the waters are characterized by an enrichment in trace elements (e.g. Cs, Li, Sb, As, B, Tl, and Rb), which are an useful tool for a better understanding of the processes affecting the waters, as well as providing valuable insight into the quality of the water and the potential for its exploitation.

The thermal waters feed the rivers Manchana Covunco, Aguas Calientes, and Covunco rivers, which turn their compositions from Na^+/Ca^{2+}-HCO_3^- to Na^+-Cl^-, and, as consequence, the main river, Varvarco river, which shifts its compositions from Ca^{2+}-SO_4^{2-}(HCO_3^-) to Na^+/Ca^{2+}-Cl^-(SO_4^{2-}). The rivers fed by thermal waters and the Varvarco rivers result in elevated concentrations of minor species such as Cs, Li, Sb, As, B, Tl, and Rb. The mass fluxes of trace elements to the Varvarco river are elevated and range between 45 and 278 t y^{-1} for B, As, Rb, and Cs, and between 0.3 and 3 t y^{-1} for Tl and Sb, increasing one to two orders of magnitude its fluxes in the Varvarco river, and reaching concentrations above 0.1 mg L^{-1} also for toxic elements such as As (Villalba et al., 2020). The RMs and fluxes of trace elements almost do not change through time in most waters. Nevertheless, these contributions were defined during the end of the summer, where the snow melt is almost finished, therefore the streamflow is lower (Falaschi et al., 2022) and can have an impact on the measured concentrations, but not on the calculated fluxes. Finally, it is important to mention that this is an active volcanic system, where the input of magmatic gases to the geothermal manifestations can increase, enriching the waters in some element concentrations and their fluxes through the rivers.

4. Conclusions

In this study, we present new unpublished data on the hydrological system of the Domuyo Volcanic Complex, one of the most promising geothermal systems in Argentina. Thirty-eight surface water samples from 17 different sites, including cold and hot springs, bubbling pools, the main river and its tributaries, were sampled between 2013 and 2016 and major dissolved ions and trace elements were analysed. A reevaluation of the total energy output of the system was calculated obtaining an average value of 1.0 ± 0.2 GW, representing an impressive advective heat flux that confirms that it is one of the most impressive geothermal systems in the world. Using the new trace element dataset, it was possible to integrate and refine the hydrogeochemical model already proposed by previous authors. The main processes governing the chemical composition of thermal springs (40–97 °C) include: i) shallow water-rock interaction processes; ii) deep magmatic input to the geothermal brine providing As, B, Sb, and Tl; and iii) progressive rock leaching in the mature geothermal system that provides Li, Cs, and Rb to the brine. The thermal springs feed the rivers that drain through the geothermal field, substantially modifying their compositions by increasing concentrations and flow rates of many trace elements. All these small rivers are tributaries of the main watercourse, the Varvarco River, where the geothermal input is clearly reflected in its chemical composition. During the three years of monitoring, the fluxes of Li, Cs, Rb, As, B, Sb, and Tl in the Varvarco downstream were much higher (up to two orders of magnitude) than in the Varvarco upstream. These new results highlight two important aspects: on one hand, the geothermal system has enormous potential for geothermal exploitation, and also for the potential supply of strategic industrial elements such as B (~ 278 t y^{-1}) and Li (~ 380 t y^{-1}), linked directly to high technology and clean energy, and other technology-critical elements including Cs (~ 49 t y^{-1}), Sb (~ 3 t y^{-1}), Co and Y (~ 0.02 and ~ 0.005 t y^{-1} respectively); on the other hand, the environmental impact should be seriously assessed considering the large quantities of potentially toxic elements released into the hydrological system, such as F (~ 118 t y^{-1}), As (~ 59 t y^{-1}), Tl (~ 0.33 t y^{-1}), Cd, Cr, Ni, Pb, and V (ranging from 0.01 to 0.08 t y^{-1}). The Domuyo Volcanic Complex is therefore an important potential economic resource, but also a potential risk as a cause of environmental pollution of the surrounding area.

CRediT authorship contribution statement

Joaquin Llano: Writing – review & editing, Writing – original draft, Visualization, Investigation, Data curation. **Lorenza Li Vigni:** Writing – review & editing, Writing – original draft, Conceptualization. **Mariano Agusto:** Writing – review & editing, Supervision, Methodology, Investigation, Conceptualization. **Lorenzo Brusca:** Writing – review & editing, Formal analysis. **Alberto Caselli:** Writing – review & editing, Investigation, Conceptualization. **Giovanni Chiodini:** Writing – review & editing, Methodology, Investigation, Data curation, Conceptualization. **Walter D'Alessandro:** Writing – review & editing, Methodology, Formal analysis. **Matteo Lelli:** Writing – review & editing, Investigation, Formal analysis. **Franco Tassi:** Writing – review & editing, Methodology, Investigation. **Orlando Vaselli:** Writing – review & editing, Methodology, Investigation. **Sergio Calabrese:** Writing – review & editing, Writing – original draft, Methodology, Investigation, Data curation, Conceptualization.

Declaration of competing interest

The authors declare that they have no known competing financial interests or personal relationships that could have appeared to influence the work reported in this paper.

Appendix A. Supplementary data

Supplementary data to this article can be found online at https://doi.org/10.1016/j.jvolgeores.2025.108322.

Data availability

The data are shared as Supplementary Materials

References

Aiuppa, A., Dongarrà, G., Capasso, G., Allard, P., 2000. Trace elements in the thermal waters of Vulcano Island. J. Volcanol. Geotherm. Res. 98, 189–207.
Aiuppa, A., D'Alessandro, W., Federico, C., Palumbo, B., Valenza, M., 2006. The aquatic geochemistry of arsenic in volcanic groundwaters from southern Italy. Appl. Geochem. 18, 1283–1296.
Arnórsson, S., Andrésdóttir, A., 1995. Processes controlling the distribution of boron and chlorine in natural waters in Iceland. Geochim. Cosmochim. Acta 59 (20), 4125–4146.
Astort, A., Walter, T.R., Ruiz, F., Sagripanti, L., Nacif, A., Acosta, G., Folguera, A., 2019. Unrest at Domuyo volcano, Argentina, detected by geophysical and geodetic data and morphometric analysis. Remote Sens. 11, 2175.
Burns, W.M., Jordan, T.E., Copeland, P., Kelley, S.A., 2006. The case for extensional tectonics in the Oligocene-Miocene Southern Andes as recorded in the Cura Mallín basin (36°-38°S). In: Kay, S.M., Ramos, V.A. (Eds.), Evolution of an Andean Margin,

A Tectonic and Magmatic View from the Andes to the Neuquén Basin (35°-39°S lat.), 407. Geological Society of America Special Papers, pp. 163–184.
Calabrese, S., Aiuppa, A., Allard, P., Bagnato, E., Bellomo, S., Brusca, L., D'Alessandro, W., Parello, F., 2011. Atmospheric sources and sinks of volcanogenic elements in a basaltic volcano (Etna, Italy). Geochim. Cosmochim. Acta 75 (23), 7401–7425.
Chiodi, A., Tassi, F., Báez, W., Filipovich, R., Bustos, E., Galli, M.G., Suzaño, N., Ahumada, M.F., Viramonte, J.G., Giordano, G., Pecoraino, G., Vaselli, O., 2019. Preliminary conceptual model of the Cerro Blanco caldera-hosted geothermal system (Southern Puna, Argentina): Inferences from geochemical investigations. J. S. Am. Earth Sci. 94, 102213.
Chiodi, A., Báez, W., Tassi, F., Bustos, E., Filipovich, R., Murray, J., Rizzo, A.L., Vaselli, O., Giordano, G., Viramonte, J.G., 2024. Fluid geochemistry of the Cerro Galán geothermal system (Southern Puna, Argentina): Implications for the geothermal potential of one of the youngest giant calderas in the Andes. J. Volcanol. Geotherm. Res. 450, 108089.
Chiodini, G., Liccioli, C., Vaselli, O., Calabrese, S., Tassi, F., Caliro, S., Caselli, A.T., Agusto, M., D'Alessandro, W., 2014. The Domuyo volcanic system: an enormous geothermal resource in Argentina Patagonia. J. Volcanol. Geotherm. Res. 274, 71–77.
Deely, J.M., Sheppard, D.S., 1996. Whangaehu River, New Zealand: geochemistry of a river discharging from an active crater lake. Appl. Geochem. 11 (3), 447–460.
D'Elia, L., Páez, G., Hernando, I.R., Petrinovic, I.A., López, L., Kürten, G., Vigiani, L., 2020. Hydrothermal eruptions at El Humazo, Domuyo geothermal field, Argentina: Insights into the eruptive dynamics and controls. J. Volcanol. Geotherm. Res. 393, 106786.
Delmelle, P., Bernard, A., 2000. Downstream composition changes of acidic volcanic waters discharged into the Banyupahit stream, Ijen caldera, Indonesia. J. Volcanol. Geotherm. Res. 97 (1–4), 55–75.
Derauw, D., Jaspard, M., Caselli, A., Samsonov, S., 2020. Ongoing automated ground deformation monitoring of Domuyo-Laguna del Maule area (Argentina) using Sentinel-1 MSBAS time series: Methodology description and first observations for the period 2015–2020. J. S. Am. Earth Sci. 104, 102850.
Ellis, A., Mahon, W., 1964. Natural hydrothermal systems and experimental hot-water/rock interactions. Geochim. Cosmochim. Acta 28 (8), 1323–1357.
Ellis, A., Mahon, W., 1967. Natural hydrothermal systems and experimental hot water/rock interactions (Part II). Geochim. Cosmochim. Acta 31 (4), 519–538.
Falaschi, D., Berthier, E., Belart, J.M., Bravo, C., Castro, M., Durand, M., Villalba, R., 2022. Increased mass loss of glaciers in Volcán Domuyo (Argentinian Andes) between 1962 and 2020, revealed by aerial photos and satellite stereo imagery. J. Glaciol. 69 (273), 40–56.
Fournier, R.O., White, D.E., Truesdell, A.H., 1976. Convective heat flow in Yellowstone National Park. Proc. Un Symp. Dev. And Use of Geotherm. Resour., San Francisco, 1975. 1: 731–39. U.S. Govt. Prin. Off, Washington, D.C.
Galetto, A., García, V., Caselli, A., 2018. Structural controls of the Domuyo geothermal field, southern Andes (36° 38′ S), Argentina. J. Struct. Geol. 114, 76–94.
Giammanco, S., Ottaviani, M., Valenza, M., Veschetti, E., Principio, E., Giammanco, G., Pignato, S., 1998. Major and trace elements geochemistry in the ground waters of a volcanic area: Mount Etna (Sicily, Italy). Water Res. 32 (1), 19–30.
Giggenbach, W.F., 1988. Geothermal solute equilibria. Derivation of Na–K–Mg–Ca geoindicators. Geochim. Cosmochim. Acta 52, 2749–2765.
Giggenbach, W.F., 1991. Chemical techniques in geothermal exploration. In: D'Amore, F. (Ed.), Application of Geochemistry in Geothermal Reservoir Development. UNITAR, New York, pp. 119–144.
Godoy, L.B., Nacif, S., Lupari, M., García, H.P., Correa-Otto, S., Melchor, I., Pechuan, S., Ariza, J.P., Gimenez, M., Caselli, A.T., 2021. Geophysical evidence of first stages of inflation in Domuyo volcanic center in northwestern Neuquén province, Argentina. J. S. Am. Earth Sci. 107, 102694.
Godoy, L.B., Nacif, S., Nacif, A., Christiansen, R., Álvarez, O., Gimenez, M., Folguera, A., 2023. Sudden alteration in the seismic behavior of the Domuyo volcanic complex in the southern volcanic backarc zone, Argentina. J. Volcanol. Geotherm. Res. 444, 107956.
Groeber, P., 1947. Observaciones geologicas a lo largo del meridian 70.3, hojas Domuyo, Mari Mahuida, Huarhuar Co y parte de Epu Lauken. Rev. Asoc. Geol. Argent. 2 (4), 347–408.
Inostroza, M., Moune, S., Moretti, R., Bonifacie, M., Robert, V., Burtin, A., Chilin-Eusebe, E., 2022. Decoding water-rock interaction and volatile input at La Soufriere volcano (Guadeloupe) using time-series major and trace element analyses in gas condensates. J. Volcanol. Geotherm. Res. 425, 107517.
JICA, Japan International Cooperation Agency, 1983. Argentine Republic. Final Report on the Northern Neuquen Geothermal Development Project. First-Second Phase Survey, N, p. 25.
JICA, Japan International Cooperation Agency, 1984. Argentine Republic. Final Report on the Northern Neuquen Geothermal Development Project. Third Phase Survey, N, p. 25.
JICA, Japan International Cooperation Agency, 1992. Report on the Northern Neuquén Geothermal development project. International cooperation Agency. Ente Provincial de Energía de la Provincia de Neuquén. Project. Final Report, 89.
Kaasalainen, H., Stefánsson, A., 2012. The chemistry of trace elements in surface geothermal waters and steam, Iceland. Chem. Geol. 330, 60–85.
Kalacheva, E., Taran, Y., Kotenko, T., 2015. Geochemistry and solute fluxes of volcano-hydrothermal systems of Shiashkotan, Kuril Islands. J. Volcanol. Geotherm. Res. 296, 40–54.
Kalacheva, E., Taran, Y., Voloshina, E., Inguaggiato, S., 2017. Hydrothermal system and acid lakes of Golovnin caldera, Kunashir, Kuril Islands: Geochemistry, solute fluxes and heat output. J. Volcanol. Geotherm. Res. 346, 10–20.
Li Vigni, L., Daskalopoulou, K., Calabrese, S., Kyriakopoulos, K., Bellomo, S., Brusca, L., Brugnone, F., D'Alessandro, W., 2023. Characterization of trace elements in thermal and mineral waters of Greece. Environ. Sci. Pollut. Res. 30, 78376–78393.
Llambías, E.J., 1986. Intrusivos pérmicos del sur de la Cordillera del Viento, provincia del Neuquén. Rev. Asoc. Geol. Argent. 41, 22–32.
Llano, J., Nogués, V., Agusto, M., Lamberti, M.C., Sierra, D., García, S., Carbajal, F., Calabrese, S., D'Alessandro, W., 2022. Geoquímica de las aguas vinculadas al Complejo Volcánico Planchón-Peteroa, Mendoza-Argentina. Rev. Asoc. Geol. Argent. 79 (3), 429–448.
Llano, J., Calabrese, S., Lamberti, M.C., Li Vigni, L., Brugnone, F., Sierra, D., García, S., Carbajal, F., Brusca, L., D'Alessandro, W., Agusto, M., 2023. Hydrogeochemistry of trace and rare earth elements in the Caviahue-Copahue Volcanic complex. Chem. Geol. 634, 121602.
Lundgren, P., Girona, T., Bato, M.G., Realmuto, V.J., Samsonov, S., Cardona, C., Franco, L., Gurrola, E., Aivazis, M., 2020. The dynamics of large silicic systems from satellite remote sensing observations: the intriguing case of Domuyo volcano, Argentina. Sci. Rep. 10 (1), 1–15.
Mandon, C.L., Christenson, B.W., Schipper, C.I., Seward, T.M., Garaebiti, E., 2019. Metal transport in volcanic plumes: a case study at White Island and Yasur volcanoes. J. Volcanol. Geotherm. Res. 369, 155–171.
Marini, L., Cioni, R., 1985. A chloride method for the determination of the enthalpy of steam/water mixtures discharged form geothermal wells. Geothermics 14 (1), 29–34.
Mas, G.R., Bengochea, L., Mas, L.C., 2000. Hydrothermal Alteration at El Humazo Geothermal Area, Domuyo Volcano, Argentina. In: Proceedings of the World Geothermal Congress, pp. 1413–1418.
Miranda, F.J., 1996. Caracterización petrográfica y geoquímica del Cerro Domuyo, Pcia. De Neuquén - Argentina [Licenciatura Thesis].. In: Buenos Aires. Universidad de Buenos Aires, Buenos Aires, Facultad de Ciencias Exactas y Naturale, p. 118.
Morales-Simfors, N., Bundschuh, J., Herath, I., Inguaggiati, C., et al., 2020. Arsenic in Latin America: a critical overview on the geochemistry of arsenic originating from geothermal features and volcanic emissions for solving ita environmental consequences. Sci. Total Environ. 716, 135564.
Panarello, H., 2002. Características isotópicas y termodinámicas de reservorio del campo geotérmico Copahue-Caviahue, provincia de Neuquén. Rev. Asoc. Geol. Argent. 57, 182–194.
Panarello, H., Sierra, J.L., Pedro, G., D'Amore, F., 1992. Isotopic and Geochemical Study of the Domuyo Geothermal Field, Neuquén. Argentina No. IAEA-TECDOC—641.
Peralta Arnold, Y., Cabassi, J., Tassi, F., Caffe, P.J., Vaselli, O., 2017. Fluid geochemistry of a deep-seated geothermal resource in the Puna plateau (Jujuy Province, Argentina). J. Volcanol. Geotherm. Res. 338, 121–134.
Pesce, A.H., 1981. Estratigrafía de las nacientes del río Neuquén y Nahuever, Provincia del Neuquén. Congreso Geol. Argentino. 3, 439–455.
Pesce, A.H., 1983. Evaluación geotérmica del área del cerro Domuyo (Neuquén), SEGEMAR (Servicio Geológico Minero Argentino) Argentina Open-File Report, Serie Contribuciones Técnicas. Geotermia 1, 46.
Pesce, A.H., 2013. The Domuyo geothermal area, Neuquén, Argentina. Geotherm. Res. Council 37, 309–314.
Rojas, A., Sruoga, P., Lamberti, M.C., Agusto, M., Tondreau, J., Mendoza, N., Daniele, L., Morata, D., 2022. Unravelling the hydrothermal system of Laguna del Maule restless volcanic field, in the Andean Southern Volcanic Zone (36° 10′ S). J. Volcanol. Geotherm. Res. 424, 107498.
Rouwet, D., Bellomo, S., Brusca, L., Inguaggiato, S., Jutzeler, M., Mora, R., Mazot, A., Bernard, R., Cassidy, M., Taran, Y., 2009. Major and trace element geochemistry of El Chichón volcano-hydrothermal system (Chiapas, México) in 2006-2007: implications for future geochemical monitoring. Geofis. Int. 48 (1), 55–72.
Scholtysik, R., Canil, D., 2018. Condensation behaviour of volatile trace metals in laboratory benchtop fumarole experiments. Chem. Geol. 492, 49–58.
Silva-Fragoso, A., Ferrari, L., Norini, G., Orozco-Esquivel, T., Corbo-Camargo, F., Bernal, J.P., Castro, C., Arrubarrena-Moreno, M., 2021. Geology and conceptual model of the Domuyo geothermal area, northern Patagonia, Argentina. J. Volcanol. Geotherm. Res. 420, 107396.
Smith, C.L., Ficklin, W.H., Thompson, J.M., 1987. Concentrations of arsenic, antimony, and boronin steam and steam condensate at the Geysers, California. J. Volcanol. Geotherm. Res. 32 (4), 329–341.
Stern, C., 2004. Active Andean volcanism: its geologic and tectonic setting. Rev. Geol. Chile 31, 161–206.
Symonds, R., Reed, M., Rose, W., 1992. Origin, speciation, and fluxes of trace element gases at Augustine volcano, Alaska – insights into magma degassing and fumarolic processes. Geochim. Cosmochim. Acta 56, 633–657.
Taran, Y., Rouwet, D., Inguaggiato, S., Aiuppa, A., 2008. Major and trace element geochemistry of neutral and acidic thermal springs at El Chichón volcano, Mexico: implications for monitoring of the volcanic activity. J. Volcanol. Geotherm. Res. 178 (2), 224–236.
Tardani, D., Roulleau, E., Pinti, D.L., Peréz-Flóres, P., Daniele, L., Reich, M., Sanchez-Alfaro, P., Morata, D., Richard, L., 2021. Structural control on shallow hydrogeochemical processes at Caviahue-Copahue Volcanic complex (CCVC), Argentina. J. Volcanol. Geotherm. Res. 414, 107228.
Tassi, F., Liccioli, C., Agusto, M., Chiodini, G., Vaselli, O., Calabrese, S., Pecoraino, G., Tempesti, L., Caponi, C., Fiebig, J., Caliro, S., Caselli, A., 2016. The hydrothermal system of the Domuyo volcanic complex (Argentina): a conceptual model based on new geochemical and isotopic evidences. J. Volcanol. Geotherm. Res. 328, 198–209.
Villalba, E., Tanjal, C., Borzi, G., Páez, G., Carol, E., 2020. Geogenic arsenic contamination of wet-meadows associated with a geothermal system in an arid region and its relevance for drinking water. Sci. Total Environ. 720, 137571.

Villalba, E., Santucci, L., Borzi, G., Pasquini, A.I., Páez, G., Carol, E., 2022. Geothermal influence on the hydrochemistry of surface streams in Patagonia Neuquina. In: Iadran Torres, A., Campodomenico, V. (Eds.), Environmental Assessment of Patagonia`s Water Resources. Springer International Publishing, Berlin Heidelberg, pp. 57–73.

Wedepohl, K.H., 1995. The composition of the continental crust. Geochim. Cosmochim. Acta 59 (7), 1217–1232.

Wrage, J., Tardani, D., Reich, M., Daniele, L., Arancibia, G., Cembrano, J., Sánchez-Alfaro, P., Morata, D., Pérez-Moreno, R., 2017. Geochemistry of thermal waters in the Southern Volcanic Zone, Chile - Implications for structural controls on geothermal fluid composition. Chem. Geol. 466, 545–561.

Zanettini, J.C., Santamaría, G.R., Leanza, H.A., 2001. Geological Chart of the Argentine Republic E. 1:250,000 num. 3772-II (Las Ovejas) Province of Neuquén. 263. Institute of Geology and Mineral Resources, Argentine Mining Geological Service. Ministry of Mining Secretariat, Argentina. Bulletin, p. 61.

Zappettini, E.O., Chernicof, C.J., Santos, J.O.S., Dalponte, M., Belousova, E., McNaughton, N., 2012. Retrowedge-related Carboniferous units and coeval magmatism in the North-Western Neuquén province, Argentina. Int. J. Earth Sci. 101, 2083–2104.

Zelenski, M., Malik, N., Taran, Y., 2014. Emissions of trace elements during the 2012-2013 effusive eruption of Tolbachik volcano, Kamchatka: enrichment factors, partition coefficients and aerosol contribution. J. Volcanol. Geotherm. Res. 285, 136–149.